Liquid Crystals
Publication details, including instructions for authors and subscription information:
http://www.informaworld.com/smpp/title~content=t713926090

Orientational relationship among main and side chains of a polyimide alignment layer, liquid crystals monolayer and bulk pretilt angle

Takahiro Sakai; Ken Ishikawa; Hideo Takezoe

Online publication date: 11 November 2010

To cite this Article Sakai, Takahiro , Ishikawa, Ken and Takezoe, Hideo(2002) 'Orientational relationship among main and side chains of a polyimide alignment layer, liquid crystals monolayer and bulk pretilt angle', Liquid Crystals, 29: 1, 47 — 55
To link to this Article: DOI: 10.1080/02678290110091653
URL: http://dx.doi.org/10.1080/02678290110091653

LIQUID CRYSTALS, 2002, VOL. 29, NO. 1, 47–55

Orientational relationship among main and side chains of a polyimide alignment layer, liquid crystals monolayer and bulk pretilt angle

TAKAHIRO SAKAI, KEN ISHIKAWA and HIDEO TAKEZOE*

Department of Organic and Polymeric Materials, Tokyo Institute of Technology, O-okayama, Meguro-ku, Tokyo 158-8552, Japan

(*Received 22 March 2001; accepted 4 June 2001*)

We have determined the orientational distribution of cyano-substituted side chains of a rubbed polyimide film, and a liquid crystal monolayer adsorbed on the film, by means of optical second harmonic generation. With the orientational distribution of a main chain that was measured in a previous study by means of near-edge X-ray absorption fine structure (NEXAFS) spectroscopy, we have obtained the correlation of all the orientational distributions contributing to the alignment of LC molecules, i.e. pretilt angle. We find that the side chain plays a role in increasing the pretilt angle, but in the case of rubbing strength dependence, the main chain has stronger correlation with the pretilt angle than has the side chain.

1. Introduction

The mechanism of the alignment of a liquid crystal (LC) on rubbed polymer surfaces is one of the most important issues from both the fundamental and industrial viewpoints. Generally, LC molecules are aligned by rubbing a substrate surface coated with polyimide (PI). This treatment induces a so-called pretilt angle defined as the tilt angle of the director with respect to the substrate surface. Since the performance of a LC display is affected by the pretilt angle, its control is one of the most significant issues in LC industries. It is well known that the pretilt angle is strongly influenced by the surface of a rubbed polymer. Accordingly, much effort has been made in the study of such surface alignment layers. However, there is still extensive argument for the mechanism of surface alignment without any successful definite explanation.

One of the powerful methods for investigating surface molecular alignment is second harmonic generation (SHG), allowing us to probe just a surface because of its surface activity due to a symmetry requirement. This technique has been applied in studying the orientations of LC monolayers [1–9] and PI alignment layers [10–19]. Furthermore, the use of SHG interferometry enables us to determine both the orientations of a SHG-active PI film and a SHG-active LC monolayer on the PI film [11, 13, 19]. Shirota and co-workers reported that the orientations of a side chain of a PI film and of a LC monolayer on it are quite different, and that serious changes in these orientations occur at the same rubbing strength, where the pretilt angle also shows a remarkable change [11]. Recently, Oh-e *et al.* also applied this technique to the surface of a main chain type PI film and mentioned the correlation between the orientations of the main chain and a LC monolayer on it [19].

Near-edge X-ray absorption fine structure (NEXAFS) spectroscopy is also a powerful tool for studying the orientation of functional groups of organic molecules at surfaces [20]. X-ray absorption leads to the emission of electrons, of such a small escape depth that the NEXAFS method supplies a surface sensitive tool. NEXAFS spectroscopy has a polarization dependence for polarized incident X-rays due to the anisotropy of transition dipole moments. Thus, the analysis of the dependence of resonance intensity on angle of incidence in the polarized spectra gives information of the molecular orientation. In previous reports by the groups of Ouchi [21, 22], Stöhr [23–25] and Wöll [26], much effort was described on surface studies of various PIs by NEXAFS. These studies revealed the preferred molecular orientation at the surface of rubbed polymer films, and concluded that this orientation is the microscopic origin for LC alignment on the surface.

For elucidation of the alignment mechanism, it is necessary to know all the molecular orientations of the main and side chains of the PI and of the LC monolayer

*Author for correspondence;
e-mail: htakezoe@occ.titech.ac.jp

Liquid Crystals ISSN 0267-8292 print/ISSN 1366-5855 online © 2002 Taylor & Francis Ltd
http://www.tandf.co.uk/journals
DOI: 10.1080/02678290110091653

on the PI film, and the bulk pretilt angle of the LC. However, there has been no report describing all these orientations and their correlations until now. Previously, we determined the orientation of the main chain of the PI used in this study by using NEXAFS spectroscopy, and the bulk pretilt angle of the same LC under the same conditions [27]. Here, we report the surface orientations of both PI side chain and the LC monolayer on the PI film under various rubbing conditions by means of SHG measurements. From these results, we discuss the correlation between these surface orientations and the bulk pretilt angle in LC cell in contact with the rubbed PI surfaces.

2. Experimental

The alignment layer used in this study was a PI copolymer called CP7CC3, which consists of two units with and without side chains (70 : 30), as shown in figure 1. The side chain contains a cyano biphenyl group which gives rise to SHG activity. The PI films were prepared by spin coating on fused quartz plates, and rubbed by a commercial rubbing machine (EHC CO., Ltd., RM-50), under the following conditions: the translation speed of the sample was 3.6 mm s^{-1}; the rotation speed of the roller was 900 rpm; the pile impression depth P_{rub} was varied between 0.2 and 0.5 mm for controlling the rubbing strength. The LC used was 5CB supplied by Merck Japan Ltd., the chemical structure of which is shown in figure 1. The LC was heated on a hot plate at 90°C for 60 min and the vapour was adsorbed on the PI surface that was located 4 cm above the hot plate. It is known that the first liquid crystal layer adsorbed on surface has a polar order [13], resulting in an SHG-active layer. Further evaporation gives rise to negligible increase of SHG intensity, suggesting head–tail orientation.

The SHG and its interferometry experiments were conducted using the optical set-up described in our previous work [11, 12]. The light source ($\lambda = 532$ nm) was obtained from a Q-switched Nd : YAG laser (DCR-11, Quanta-Ray) with a frequency doubler (HG-II, Quanta-Ray). The

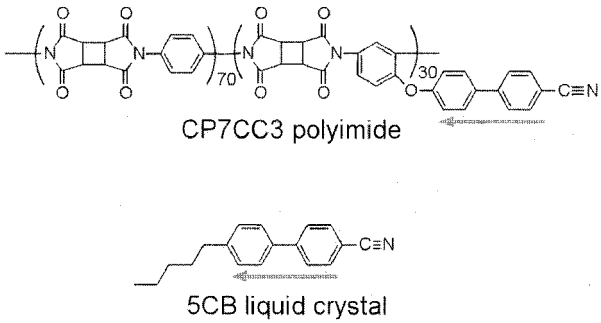

Figure 1. Chemical structures of CP7CC3 polyimide molecular unit and 5CB liquid crystal. Arrows indicate the direction of non-linear polarization responsible for SHG.

incident fundamental beam was directed onto the sample at a 45° angle of incidence after selecting the polarization of the incident beam. The SH intensity from the sample was measured as a function of sample rotation angle Φ for four different input and output polarization combinations: p-in/p-out, p-in/s-out, s-in/p-out and s-in/s-out. The theory for determining the non-linear susceptibility $\chi^{(2)}$ responsible for SHG, and the orientational distribution function (ODF) from the SHG intensity measurement, has been described in detail elsewhere [14–16, 28].

Since both the PI and LC are SHG active, it is not straightforward to determine the $\chi^{(2)}$ values of both the SHG-active media. In order to deduce the $\chi^{(2)}$ values for the LC monolayer, we measured the phase difference of SHG signals from the PI sample and the LC monolayer (PI+ LC), using SHG interferometry. In this measurement, the light after passing through the sample was also cast upon a quartz plate and then blocked by two filters. The transmitted SHG signals from the sample and the quartz plate were detected using a photomultiplier tube after passing through an analyser. The SH interference pattern could be obtained by translating the quartz plate along the beam direction because of the dispersion of the refractive index of air [13]. Comparing the interference patterns from PI samples with and without the LC monolayer, we could deduce the phase difference. First, we measured the SHG intensity from the sample with only a PI film without the quartz plate to determine the $\chi^{(2)}$ values. Then, an interference pattern was obtained by inserting the quartz plate and translating it. After evaporating LC onto the PI film, the same SHG interferometry procedure was repeated.

3. Experimental results

3.1. *Orientation of rubbed polyimide layer*

The rotational angle Φ dependences of the SH intensity from the rubbed PI, CP7CC3, are shown in figure 2, where Φ is defined as zero when the rubbing direction is in the optic plane and the projection of the light propagation direction on the plane is parallel to it. The radial length shows the SH intensity. For all the polarization combinations, characteristic anisotropic patterns due to rubbing are observed. The solid curves in figure 2 show the best fitted theoretical curves, from which the orientational distribution functions (ODFs) of the PI side chains were obtained using a modified maximum entropy method [28]. The results are shown in figure 3 for three pile impression depths. The 3D graphs show ODFs, $f(\theta, \phi)$, displayed in sample coordinates (x, y, z), where the x and z axes are defined as the rubbing direction and the surface normal. Rubbing treatments were performed from $-x$ to $+x$ direction as indicated by an arrow. The 2D graphs of ODFs are contour-plots of the molecular orientational probability as a function

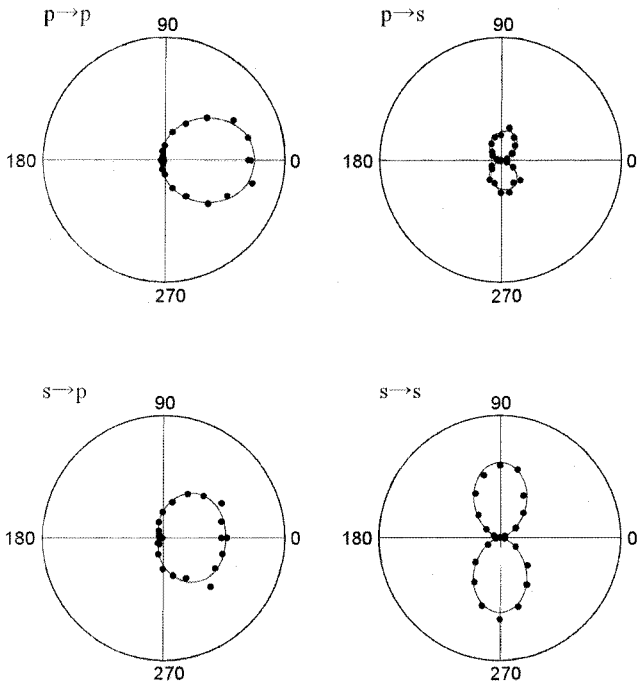

Figure 2. Polar plots of the SH signal as a function of sample rotation angle Φ in rubbed CP7CC3. The input and output polarization combinations are p-in/s-out, s-in/p-out, and s-in/s-out. Solid curves are the theoretical fit.

of θ and ϕ, where θ is the polar angle from the z axis, and ϕ is the azimuthal angle from the x axis. It is clear from the figure that the side chains align along the rubbing direction. The tilt angle showing the maximum distribution is dependent on the azimuthal angle, i.e. rubbing action tends to align the side chains toward the rubbing direction ($\phi = 0°$), so that the side chain is pushed down to $\theta = 65°$ at $\phi = 0°$ and is pulled up to $\theta = 50°$ at $\phi = 180°$. These tilt angles at $\phi = 0°$ and 180° scarcely depend on the rubbing strength. The rubbing dependence appears in the maximum value (f_{max}) of ODF, i.e., $f_{max}(\phi = 0°)$ is larger than $f_{max}(\phi = 180°)$ and the difference increases with increasing pile impression depth (rubbing strength). In fact, a small peak exists at $\phi = 180°$ under weaker rubbing strength (*a*) but disappears and the peak at $\phi = 0°$ becomes steeper under stronger rubbing stength (*c*).

3.2. *Orientation of the liquid crystal monolayer*

We now wish to know how liquid crystal molecules align on these films. First, we measured the SH intensity from the PI+ LC samples as a function of Φ. The results are shown in figure 4. The SH profiles change from those shown in figure 2 for all the polarization combinations. From this measurement, we obtained the $\chi^{(2)}_{PI+LC}$ values for a PI layer with LC on it. Second, we measured the phase differences. Figure 5 (*a*) shows the interference patterns of the p-in/p-out SHG signals from PI and (PI+ LC) samples as a function of the displacement of the quartz plate, Δl. The PI film used was rubbed under the condition of $P_{rub} = 0.5$ mm and was set at $\Phi = 0$. In both cases, the periods of these patterns were 13.8 mm, which is consistent with the calulated value. By comparing the two interference patterns, we found that the phase difference between PI and (PI+ LC) samples was 127°. Experiments were also made for the s-in/p-out signal for various Φ values in cells treated with different rubbing strengths. As expected, the phase difference between the $\chi^{(2)}_{PI}$ and $\chi^{(12)}_{PI+LC}$ is independent of factors such as the polarization combinations. The phase difference agrees with that in our previous report [13] using a homopolymer of CP7CC3 with side chains and 8CB. Thus, we obtain the ratio of the values of $\chi^{(2)}_{PI}$ and $\chi^{(2)}_{PI+LC}$ (1 : 1.55) and the phase difference between these signals. Using the relation between $\chi^{(2)}$s as shown in figure 5 (*b*), we can find the values of $\chi^{(2)}_{LC}$ for the LC monolayer as a function of Φ for all the polarization combinations.

Figure 6 shows the Φ dependences of the SH intensity of $\chi^{(2)}_{LC}$ thus calculated. From the theoretical fit and using a modified maximum entropy method [28], we find ODFs for the LC monolayer, as shown in figure 7. From the ODF plots, we notice the following characteristic features. (1) The azimuthal angle dependence becomes notable, as clearly seen from the decrease of f at $\phi = 90°$ (perpendicular to the rubbing direction) and the increase of f at $\phi = 0°$ and 180° (parallel and antiparallel to the rubbing direction, respectively) with increasing pile impression depth. This fact indicates that the LC molecules in the LC monolayer have higher orientation anisotropy along the rubbing direction as the rubbing strength increases. (2) Even at high rubbing strength, the peak at $\phi = 180°$ does not disappear, unlike ODFs in the PI side chain (see figure 3). The difference of f values at $\phi = 0°$ and 180° is rather less pronounced under stronger rubbing conditions. (3) The tilt angles showing the maximum distribution at $\phi = 0°$ and 180° are about 70° and 47°, respectively, at $P_{rub} = 0.50$; they depend slightly on the rubbing strength.

3.3. *Pretilt angle*

To compare the surface LC orientation with that in the bulk, pretilt angles were determined using the crystal rotation method. Figure 8 shows the transmittance of laser (He-Ne) light against the sample rotation angle about the axis perpendicular to the laser beam. The solid curve in the figure shows the theoretical fit, leading to a pretilt angle of 4.5° and a cell thickness of 52.3 μm. The cell thickness agrees well with that determined from the fringe pattern in a transmittance spectrum (52.5 μm).

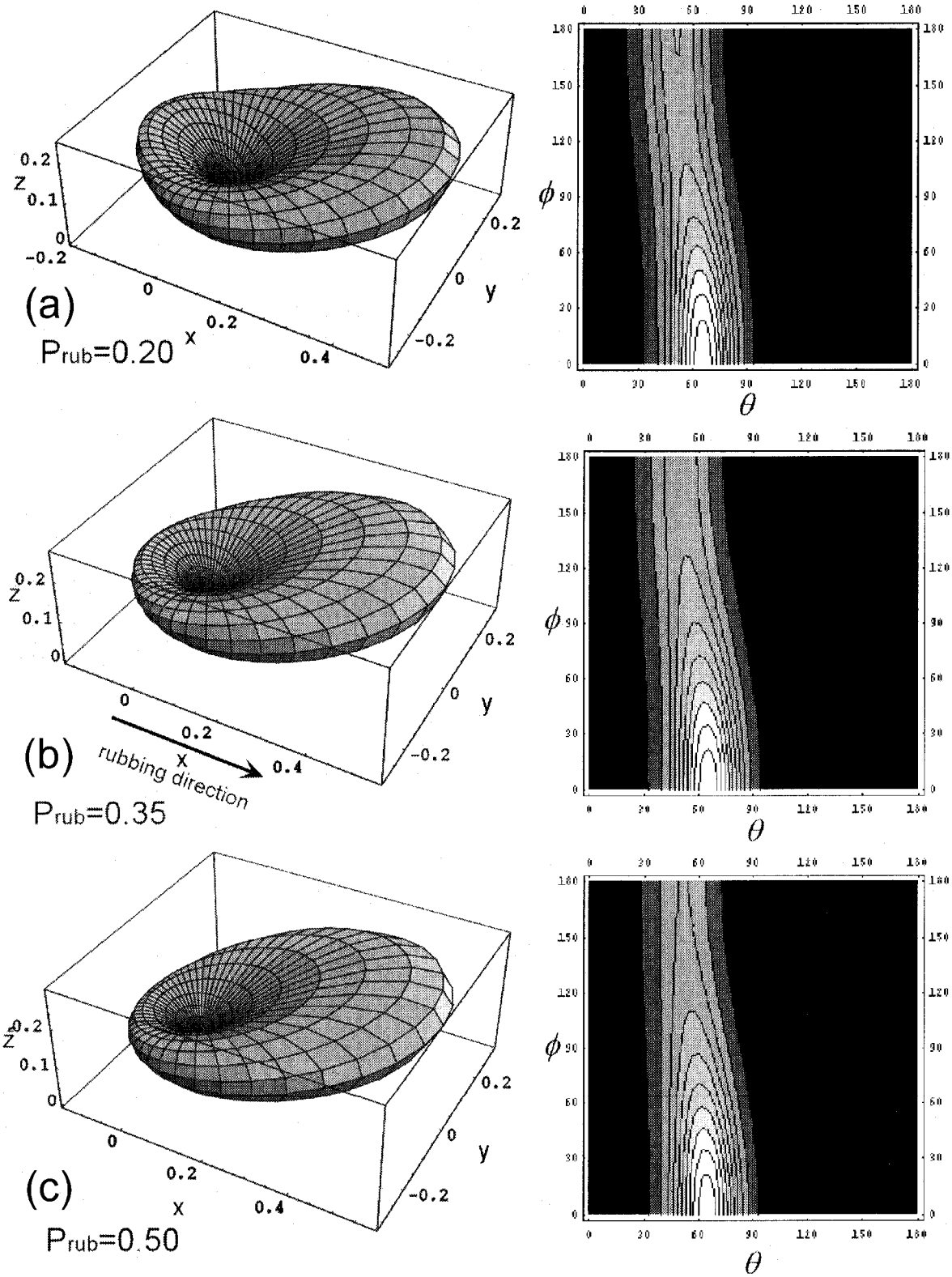

Figure 3. Orientational distribution functions, $f(\theta, \phi)$, of the side chains of the rubbed PI under different pile impression conditions: $P_{rub} =$ (*a*) 0.20 mm, (*b*) 0.35 mm and (*c*) 0.50 mm. The left side 3D maps are 3D plots in sample frame (x, y, z). The distance between the origin and each particular surface point represents the density of molecular distribution. The sample coordinate system is chosen with the rubbing direction along the x axis and the sample normal along the z axis. The right side 2D maps are contour plots of f as functions of polar θ and azimuthal ϕ angles. The rubbing direction is from 180° to 0°.

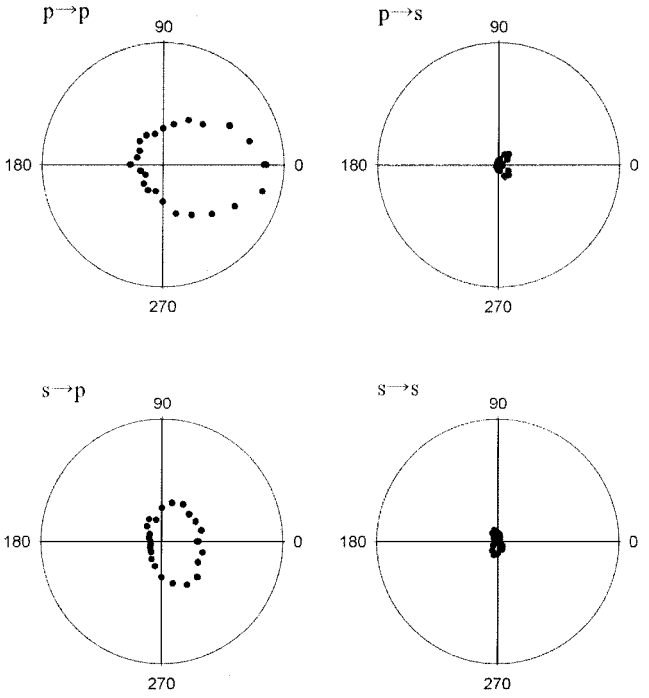

Figure 4. Polar plots of the SH signal from a rubbed PI sample with LC monolayer on it under p-in/p-out, p-in/s-out, s-in/p-out, and s-in/s-out polarization conditions.

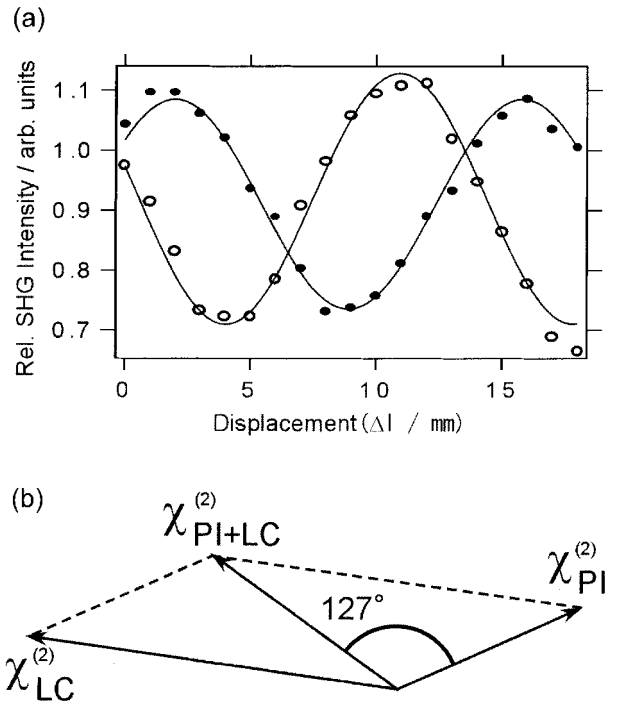

Figure 5. (*a*) SHG interference patterns obtained in p-in/p-out signal from a quartz plate and either PI film (filled circle) or PI + LC film (open circle). Solid curves represent theoretical fits, leading to a phase difference of 127°. The vertical scales for the two curves are different. (*b*) Schematic illustration of the relative amplitude and phase relation among $\chi^{(2)}_{PI}$, $\chi^{(2)}_{PI+LC}$, and $\chi^{(2)}_{LC}$. Using the vectors $\chi^{(2)}_{PI}$ and $\chi^{(2)}_{PI+LC}$ and the angle between them, we can determine $\chi^{(2)}_{LC}$.

The pretilt angle was measured in cells fabricated with CP7CC3-coated substrates rubbed antiparallel with different rubbing strengths. The rubbing strength (pile impression depth) dependence of the pretilt angle is shown in figure 9. The pretilt angle decreases with increasing rubbing strength.

4. Discussion

In this study we determined the ODFs of the side chain of CP7CC3 and of the LC monolayer on it. As for the bulk LC orientation, we only know the average orientational direction, the pretilt angle. In previous work [27], we determined the average orientation of the CP7CC3 main chain. With all this information of molecular orientations on hand, let us consider the correlation among these orientations.

In order to compare the surface orientation (ODF) of the side chain and the LC monolayer with the orientation of the main chain and the pretilt angle, we approximated the ODFs by an ellipsoidal distribution function with the average molecular orientation θ_n with respect to the rubbing direction (see figure 10). θ_n is determined by maximizing $\langle \cos^2 \alpha_N \rangle$, where α_N is the angle between the directions of molecules at the monolayer or of the side chain (N) and the director **n**; the bracket means average over the entire molecular orientational distribution. The tensor order parameter Q_{ij} [29] is written in the form

$$Q_{ij} = \begin{pmatrix} -\frac{1}{2}(S+P) & 0 & 0 \\ 0 & -\frac{1}{2}(S-P) & 0 \\ 0 & 0 & S \end{pmatrix}$$

$$= \begin{pmatrix} \frac{1}{2}(3\langle \sin^2\alpha \cos^2\varphi \rangle - 1) & 0 & 0 \\ 0 & \frac{1}{2}(3\langle \sin^2\alpha \sin^2\varphi \rangle - 1) & 0 \\ 0 & 0 & \frac{1}{2}(3\langle \cos^2\alpha \rangle - 1) \end{pmatrix}$$

$$= \begin{pmatrix} \frac{1}{2}(3f_{x'} - 1) & 0 & 0 \\ 0 & \frac{1}{2}(3f_{y'} - 1) & 0 \\ 0 & 0 & \frac{1}{2}(3f_{z'} - 1) \end{pmatrix} \quad (1)$$

where S is the uniaxial order parameter and P denotes the biaxiality; and α and φ are the polar angle from the

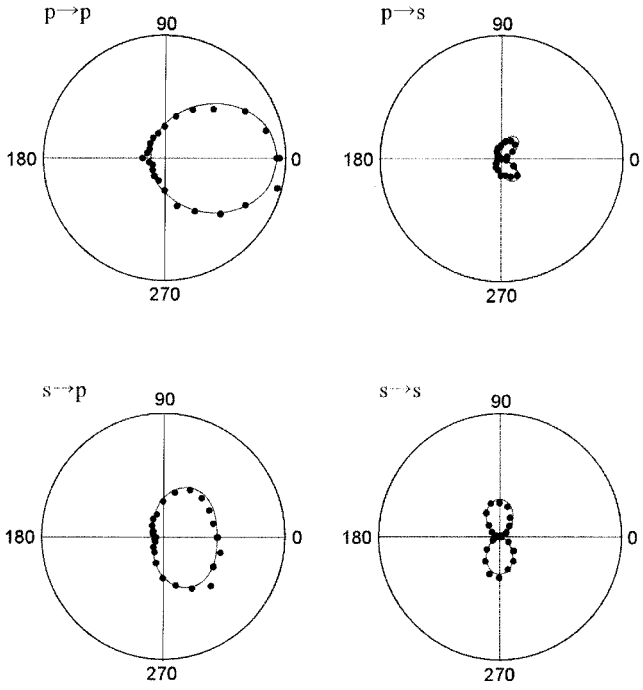

Figure 6. Deduced SH signals on an LC monolayer evaporated on the PI film as a function of sample rotation angle. The input and output polarization combinations are p-in/p-out, p-in/s-out, s-in/p-out, and s-in/s-out. Solid curves are the theoretical fit.

z' axis and the azimuthal angle form x' axis, respectively, and $f_{x'}$, $f_{y'}$ and $f_{z'}$ are so-called orientation factors and are normalized ($f_{x'} + f_{y'} + f_{z'} = 1$) [24], as shown in figure 10.

First we consider the orientation of the side chain. The parameters calculated for the side chain using the ODFs (see figure 3) are shown in table 1. The average angles for the side chains with respect to the surface are 19.8°, 25.5° and 27° for $P_{rub} = 0.2$, 0.35 and 0.5 mm, respectively. However, as shown in figures 8 and 9, the pretilt angles determined in actual cells are much smaller and show opposite dependence against the rubbing strength. Thus, the side chain orientation alone is insufficient to determine the pretilt angle.

In contrast, the molecules in the LC monolayer on CP7CC3 exhibit the opposite rubbing strength dependence to that in the side chain, as shown in table 2; thus, the angle θ_n decreases with increasing rubbing strength. The LC molecules, being in contact with rubbed CP7CC3, therefore have a totally different behaviour from that of the side chains of CP7CC3 in their rubbing strength dependence. This result suggests the important role played by the main chain of CP7CC3 for the orientation of LC molecules on this polymer.

Table 3 shows the surface tilt angle γ for the main chain determined by NEXAFS together with the pretilt angle. A strong correlation can be seen between the orientation of the main chain and the pretilt angle, as reported previously [27].

We thus obtained the ODFs of the PI side chains and LC monolayer on PI in addition to the average orientation of the main chain determined by NEXAFS and the pretilt angle of LC in the cell. The average tilt of the main chain with respect to the surface and the

Table 1. Tilt angles (θ_n) and order parameters of the side chain as a function of rubbing strength (expressed by pile impression depth P_{rub}) determined by SHG. Both uniaxial (S) and biaxial (P) order parameters are shown. f_i denotes an orientation factor along the i direction.

	Rubbing strength (pile impression/mm)		
Parameter	0.20	0.35	0.50
Tile angle of side chain θ_n/degree	19.8	25.5	27.0
S	0.139	0.172	0.197
P	0.154	0.168	0.199
$f_{x'}$	0.236	0.220	0.202
$f_{y'}$	0.338	0.332	0.334
$f_{z'}$	0.426	0.448	0.465

Table 2. Tilt angles (θ_n) and order parameters of a LC monolayer as a function of rubbing strength (expressed by pile impression depth P_{rub}) determined by SHG. Both uniaxial (S) and biaxial (P) order parameters are shown. f_i denotes an orientation factor along the i direction.

	Rubbing strength (pile impression/mm)		
Parameter	0.20	0.35	0.50
Tile angle of LC in monolayer θ_n/degree	10.0	3.4	1.6
S	0.106	0.108	0.124
P	0.072	0.140	0.080
$f_{x'}$	0.274	0.250	0.265
$f_{y'}$	0.322	0.344	0.319
$f_{z'}$	0.404	0.405	0.416

Table 3. Surface tilt angles of the main chain and pretilt angles as functions of rubbing strength (expressed by pile impression depth P_{rub}) determined by NEXAFS [27] at the C K-shell absorption edge. Pretilt angles determined by the crystal rotation method are also shown.

	Rubbing strength (pile impression/mm)		
	0.20	0.35	0.50
Surface tilt angle of main chain γ/degree	7.3	5.5	4.4
Pretilt angle/degree	7.5	5.2	4.5

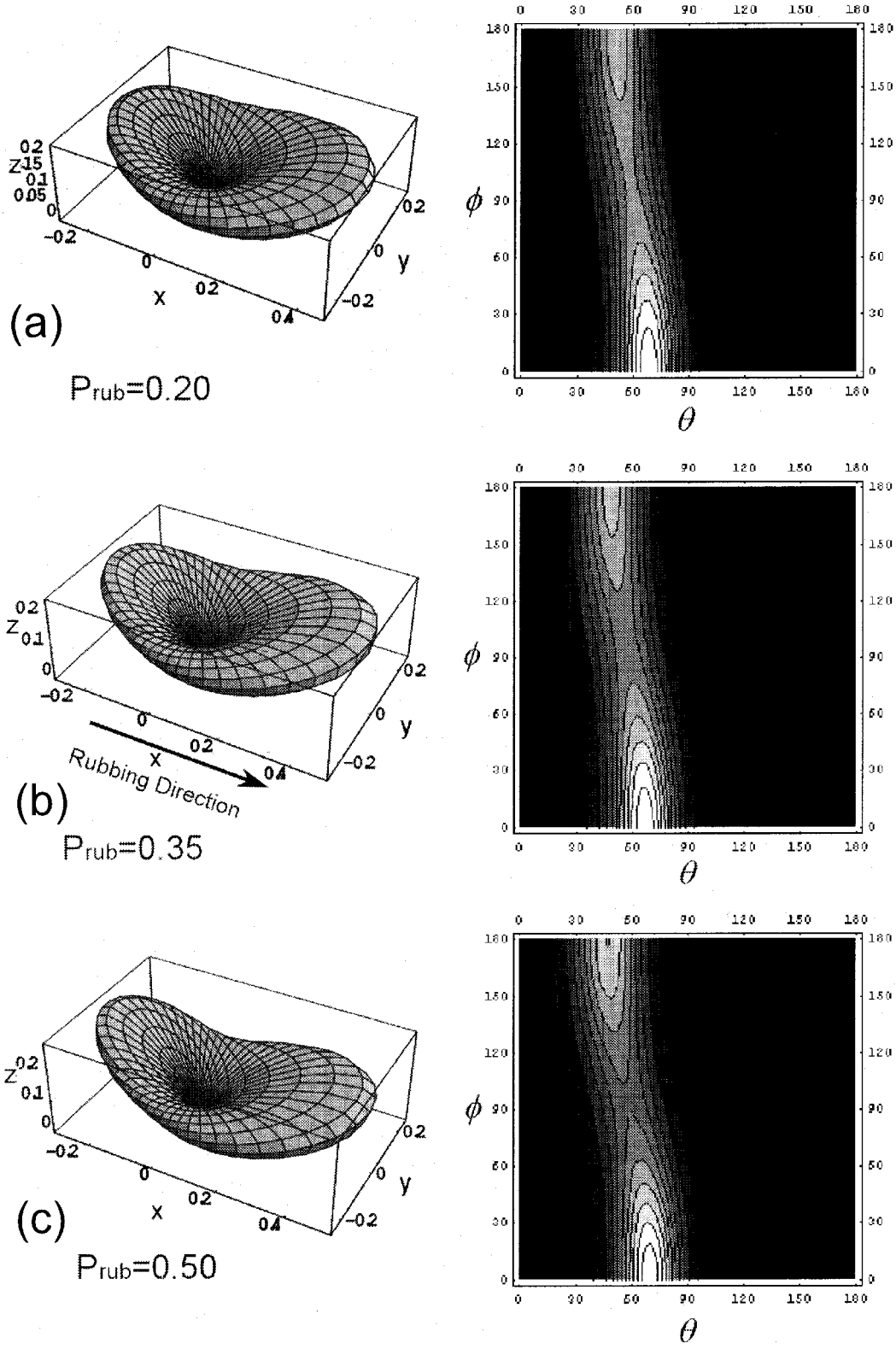

Figure 7. Orientational distribution functions, $f(\theta, \phi)$, of the LC monolayer on rubbed PI under different pile impression depth conditions: (*a*) 0.20 mm, (*b*) 0.35 mm and (*c*) 0.50 mm. The left side 3D maps are 3D plots in sample frame (x, y, z). The distance between the origin and each particular surface point represents the density of molecular distribution. The sample coordinate system is chosen with the rubbing direction along the x axis and the sample normal along the z axis. The right side 2D maps are contour plots of f as a function of polar θ and azimuthal ϕ angles. The rubbing direction is from 180° to 0°.

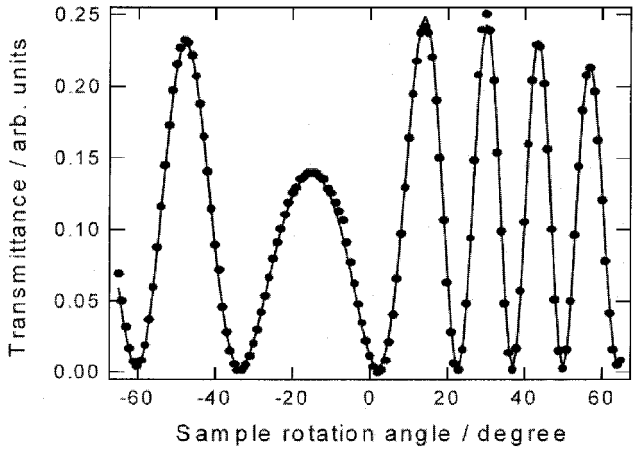

Figure 8. Transmittance signal obtained by rotating the LC cell (crystal rotation method). The solid curve represents a theoretical best fit, leading to a pretilt angle of 4.5° and a cell thickness of 52.3 μm.

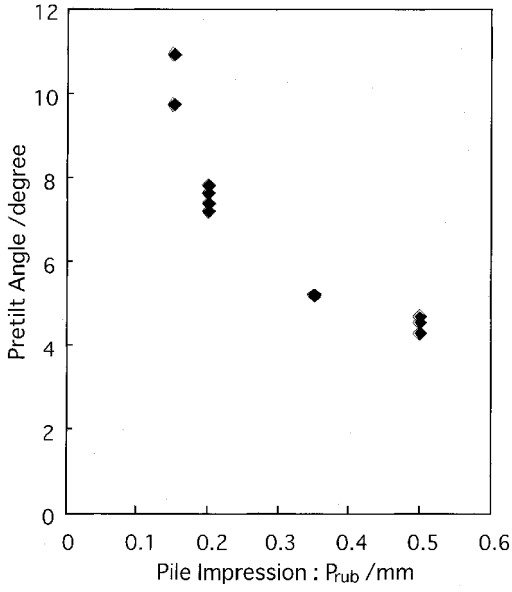

Figure 9. Rubbing strength (pile impression depth) dependence of the pretilt angle.

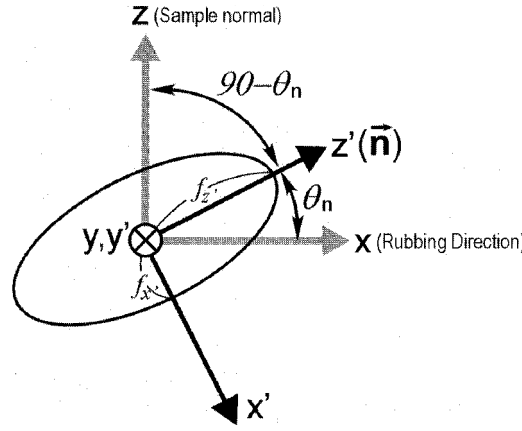

Figure 10. Ellipsoid-type distribution function and the average orientation axis (**n**) in sample coordinate system (x, y, z).

pretilt angle are well correlated, i.e. the angle decreases with increasing rubbing strength. As for the distribution of the side chain and LC monolayer on PI, ODFs obtained were approximated to ellipsoidal distributions to compare the average orientation directions with the pretilt angle. From the results, the average orientation direction of the side chain increases with increasing rubbing strength, showing an opposite rubbing strength dependence to that of the pretilt angle. This is not surprising, since the unit containing the side chain is only 30% of this copolymer, and the LC molecular orientation is also influenced by the main chain. As for the LC monolayer on PI, the average molecular orientation in the ellipsoidal model decreases with increasing rubbing strength, being consistent with the rubbing strength dependence of the pretilt angle, although quantitative agreement is not obtained. This lack of quantitative agreement may be due to the oversimplified ellipsoidal model. It is clear that the LC molecular orientation distribution is far from the ellipsoidal shape, but is that shown in figure 7. The estimation of the uniaxial molecular orientation governed by a given surface molecular orientation is a problem for the future.

5. Concluding remarks

We have investigated the surface orientation of a polyimide film with side chains using surface-sensitive SHG and its interference techniques. Rubbing-induced anisotropic distribution functions of the PI side chain and the liquid crystal monolayer on the polyimide film were determined for films treated with three different rubbing strengths. It was found that the side chains align along the rubbing direction, with the tilt angle showing a maximum distribution depending on the azimuthal angle but being independent of the rubbing strength. A rubbing dependence appears in the anisotropic orientational distribution along the rubbing direction (see figure 3). Surprisingly, the orientational distribution of the liquid crystal molecules in contact with the polyimide film is quite different (compare figures 7 and 3). The distribution maxima appear at both sides parallel and antiparallel to the rubbing direction, and increase with increasing rubbing strength. The anisotropy along the rubbing direction appears as the large difference between the tilt angles showing maximum distribution.

By approximating the complicated distributions by ellipsoidal distribution functions, the average molecular orientations of the side chain and the liquid crystal

monolayer were compared. We found that they show an opposing dependence against rubbing strength. This result clearly indicates the important role played by the main chain for liquid crystal alignment. The orientations of side chain and liquid crystal monolayer were compared with (a) pretilt angles determined using cells in contact with as-prepared substrates, and (b) the orientation of the main chain of the polyimide film determined by NEXAFS. It was found that the LC monolayer tilt angle is correlated with the surface tilt angle of the main chain even for the polyimide copolymer comprising 30% of side chains (CP7CC3), though the side chain contributes to an increase in pretilt angle.

The PI materials used in this study were supplied by Nissan Chemical Co. Ltd. One of the authors, T.S., is a Research Fellow of the Japan Society for the Promotion of Science.

References

[1] Chen, W., Feller, M. B., and Shen, Y. R., 1989, *Phys. Rev. Lett.*, **63,** 2665.
[2] Feller, M. B., Chen, W., and Shen, Y. R., 1992, *Phys. Rev.*, **43,** 6778.
[3] Barmentlo, M., van Aerle, N. A. J. M., Hollering, R. W. J., and Damen, J. P. M., 1992, *J. appl. Phys.*, **71,** 4799.
[4] Barmentlo, M., Hollering, R. W. J., and van Aerle, N. A. J. M., 1992, *Phys. Rev. A*, **46,** R4490.
[5] Barmentlo, M., Hollering, R. W. J., and van Aerle, N. A. J. M., 1992, *Liq. Cryst.*, **14,** 475.
[6] Johannsmann, D., Zhou, H., Sonderkaer, P., Wierenga, H., Myrvold, B. O., and Shen, Y. R., 1993, *Phys. Rev. E*, **48,** 1889.
[7] Zhuang, X., Marrucci, L., and Shen, Y. R., 1994, *Phys. Rev. Lett.*, **73,** 1513.
[8] Huang, J. Y., Li, J. S., Juang, Y.-S., and Chen, S.-H., 1995, *Jpn. J. appl. Phys.*, **34,** 3163.
[9] Shirota, K., Yaginuma, M., Sakai, T., Ishikawa, K., Takezoe, H., and Fukuda, A., 1996, *Jpn. J. appl. Phys.*, **35,** 2275.
[10] Shirota, K., Ishikawa, K., Takezoe, H., Fukuda, A., and Shiibashi, T., 1995, *Jpn. J. appl. Phys.*, **34,** L316.
[11] Shirota, K., Yaginuma, M., Sakai, T., Ishikawa, K., Takezoe, H., and Fukuda, A., 1996, *Appl. Phys. Lett.*, **69,** 164.
[12] Sakai, T., Yoo, J.-G., Kinoshita, Y., Ishikawa, K., Takezoe, H., and Fukuda, 1997, *Appl. Phys. Lett.*, **71,** 2274.
[13] Sakai, T., Shirota, K., Yamada, T., Hoshi, H., Ishikawa, K., Takezoe, H., and Fukuda, 1996, *Jpn. J. appl. Phys.*, **35,** 3971.
[14] Yoo, J.-G., Hoshi, H., Sakai, T., Park, B., Ishikawa, K., Takezoe, H., and Lee, Y. S., 1998, *J. appl. Phys.*, **84,** 4079.
[15] Yoo, J.-G., Park, B., Sakai, T., Kinoshita, Y., Hoshi, H., Ishikawa, K., and Takezoe, H., 1998, *Jpn. J. appl. Phys.*, **37,** 4124.
[16] Park, B., Yoo, J.-G., Sakai, T., Hoshi, H., Ishikawa, K., and Takezoe, H., 1998, *Phys. Rev. E*, **58,** 4624.
[17] Meister, R., and Jèrôme, B., 1999, *Macromolecules*, **32,** 480.
[18] Sei, M., Nagayama, H., Kajikawa, K., Ishii, H., Seki, K., Kondo, K., Matsumoto, Y., and Ouchi, Y., 1998, *Jpn. J. appl. Phys.*, **37,** 1974.
[19] Oh-e, M., Hong, S. C., and Shen, Y. R., 2000, *J. phys. Chem. B*, **104,** 7455.
[20] Stöhr, J., 1992, *NEXAFS Spectroscopy*, Vol. 25 of Springer Series in Surface Sciences (Heidelberg: Springer).
[21] Ouchi, Y., Mori, I., Sei, M., Ito, E., Araki, T., Ishii, H., Seki, K., and Kondo, K., 1995, *Physica D*, **208/209,** 407.
[22] Mori, I., Araki, T., Ishii, H., Ouchi, Y., Seki, K., and Kondo, K., 1996, *J. electron. Spectrosc. relat. Phenom.*, **78,** 371.
[23] Samant, M. G., Stöhr, J., Brown, H. R., Russel, T. P., Sands, J. M., and Kumar, S. K., 1996, *Macromolecules*, **29,** 8334.
[24] Stöhr, J., Samant, M. G., Cossy-Favre, A., Dìaz, J., Momoi, Y., Odahara, S., and Nagata, T., 1998, *Macromolecules*, **31,** 1942.
[25] Stöhr, J., and Samant, M. G., 1999, *J. electron. Spectrosc. relat. Phenom.*, **98/99,** 189.
[26] Weiss, K., Wöll, C., Böhm, E., Fiebranz, B., Forstmann, G., Peng, B., Scheumann, V., and Johannsmann, D., 1998, *Macromolecules*, **31,** 1930.
[27] Sakai, Ishikawa, K., Takezoe, H., Matsuie, N., Yamamoto, Y., Ishii, H., Ouchi, Y., Oji, H., and Seki, K., 2001, *J. phys. Chem.*, **105,** 9191.
[28] Park, B., Konoshita, Y., Sakai, T., Yoo, J.-G., Hoshi, H., Ishikawa, K., and Takezoe, H., 1998, *Phys. Rev. E*, **57,** 6717.
[29] Thulstrup, E. W., and Michl, J., 1989, *Elementary Polarization Spectroscopy* (New York: VCH).